Targeted disruption of the biglycan gene leads to an osteoporosis-like phenotype in mice

Tianshun Xu[1], Paolo Bianco[2], Larry W. Fisher[1], Glenn Longenecker[3], Erica Smith[4], Steven Goldstein[4], Jeffrey Bonadio[5], Adele Boskey[6], Anne-Marie Heegaard[1], Beatrice Sommer[1], Kazuhito Satomura[1], Pedro Dominguez[1], Chengyan Zhao[1], Ashok B. Kulkarni[3], Pamela Gehron Robey[1] & Marian F. Young[1]

The resilience and strength of bone is due to the orderly mineralization of a specialized extracellular matrix (ECM) composed of type I collagen (90%) and a host of non-collagenous proteins that are, in general, also found in other tissues. Biglycan (encoded by the gene *Bgn*) is an ECM proteoglycan that is enriched in bone[1–3] and other non-skeletal connective tissues. *In vitro* studies indicate that Bgn may function in connective tissue metabolism by binding to collagen fibrils[4] and TGF-β (refs 5,6), and may promote neuronal survival[7]. To study the role of *Bgn in vivo*, we generated *Bgn*-deficient mice. Although apparently normal at birth, these mice display a phenotype characterized by a reduced growth rate and decreased bone mass due to the absence of *Bgn*. To our knowledge, this is the first report in which deficiency of a non-collagenous ECM protein leads to a skeletal phenotype that is marked by low bone mass that becomes more obvious with age. These mice may serve as an animal model to study the role of ECM proteins in osteoporosis.

The family of small, leucine-rich proteoglycans includes biglycan, decorin, fibromodulin, lumican, epiphycan and karatocan[8]. The core proteins, to which various glycosaminoglycan side chains are covalently attached, are mainly composed of tandemly linked repeats of an approximately 25-aa leucine-rich sequence. These small proteoglycans function in matrix organization and in cell metabolism *via* binding to growth factors[8–10]. We studied the function of one member of this family, *Bgn*, by generation of *Bgn*-deficient mice using homologous recombination in embryonic stem (ES) cells (Fig. 1*a*). Two independent ES cell clones were used to produce chimaeras capable of germline transmission of the targeted allele. As *Bgn* is located on the X chromosome, wild-type mice have a genotype of $Bgn^{+/0}$ (male) and $Bgn^{+/+}$(female). Mutant male mice are $Bgn^{-/0}$ (Fig. 1*b*) and do not express *Bgn* mRNA (Fig. 1*c*) or protein (Fig. 1*d*). Conversely, the level of decorin, a related proteoglycan, was unaffected in mineralized bone matrix (Fig. 1*d*).

$Bgn^{-/0}$ mice were born with no apparent patterning defects, and grew normally until three months after birth, at which point their growth rate decreased. At six months of age, the body weight of mutant mice was significantly lower than that of wild-type littermates ($Bgn^{-/0}$ 31 ± 4.0 g, n = 11; $Bgn^{+/0}$ 41 ± 6.4 g, n = 7; $P<0.001$), but by nine months this difference had disappeared ($Bgn^{-/0}$ 37.0 ± 7.7 g, n = 11; $Bgn^{+/0}$ 41.2 ± 9.2 g, n = 7; $P = 0.167$). Although tibia from nine-month-old animals were unaffected ($Bgn^{-/0}$ 18.4 ± 0.53 mm, n = 12; $Bgn^{+/0}$ 19 ± 0.98 mm, n = 7; $P = 0.08$), femur length at six months was slightly shorter in $Bgn^{-/0}$ mice ($Bgn^{-/0}$ 15.2 ± 0.5 mm, n = 11; $Bgn^{+/0}$ 15.8 ± 0.6 mm, n = 14; $P<0.05$) and the mutant femurs became progressively shorter compared with normal littermates at nine months ($Bgn^{-/0}$ 15.1 ± 0.54 mm, n = 7; $Bgn^{+/0}$ 16.1 ± 0.6 mm, n = 12; $P<0.01$), indicating that *Bgn* is involved in the regulation of postnatal skeletal growth. Previous studies have shown that *BGN* expression level may be related to stature in humans. Patients with Turner syndrome (XO) have short stature and low levels of *BGN*, whereas patients

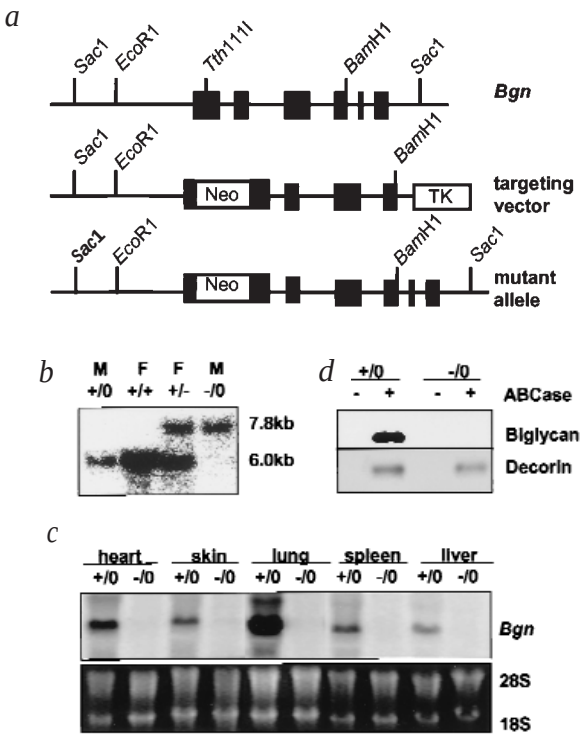

Fig. 1 Disruption of the mouse *Bgn* locus. ***a***, Schematic representation of the *Bgn* locus, gene targeting vector and recombination at the *Bgn* locus. ***b***, Representative Southern-blot analysis of male (M) and female (F) mouse tail DNA. The presence of a 7.8-kb *Sac*I fragment indicates proper targeting of the *Bgn* locus. The 6.0-kb *Sac*I fragments were from wild-type alleles. Male mice that have no second *Bgn* allele are referred to as +/0 (wild type) or –/0 (knockout). ***c***, Northern-blot analysis of RNA from $Bgn^{+/0}$ and $Bgn^{-/0}$ mice. The top panel shows the radioactivity after hybridization with *Bgn* cDNA. The bottom panel shows ethidium bromide staining of the RNA used. ***d***, Western-blot analysis of protein from skeletal tissue of mutant and wild-type littermates with or without treatment with chrondroitinase ABC (ABCase) to release the biglycan and decorin core proteins.

[1]*Craniofacial and Skeletal Diseases Branch, National Institute of Dental Research, National Institutes of Health, Bethesda, Maryland 20892, USA.* [2]*Dipartimento di Medicina Sperimentale, University of L'Aquila, 67100 L'Aquila, and University of Rome, 00161 Rome, Italy.* [3]*Gene Targeting and Research Core Facility, National Institute of Dental Research, National Institutes of Health, Bethesda, Maryland 20892, USA.* [4]*Department of Orthopaedics, University of Michigan Medical School, Ann Arbor, Michigan 48109, USA.* [5]*Department of Pathology, University of Michigan Medical School, Ann Arbor, Michigan 48109, USA.* [6]*Mineralized Tissue Research Section, The Hospital for Special Surgery, New York, New York 10021, USA. Please address all correspondence to M.F.Y., Building 30, Room 106, 30 Convent Drive MSC 4320 Bethesda, MD 20892 (e-mail: young@yoda.nidr.nih.gov).*

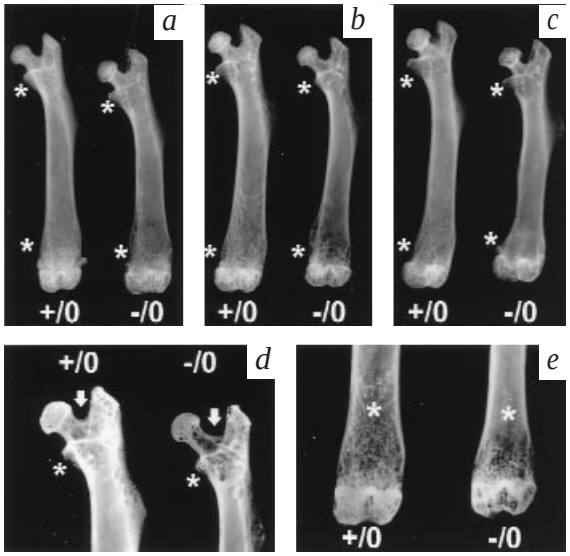

Fig. 2 Radiological analysis of bones from *Bgn*$^{+/0}$ and *Bgn*$^{-/0}$ mice. *a–c*, Radiographs of femora from wild-type (+/0) and mutant (–/0) mice at the age of three (***a***), six (***b***) and nine (***c***) months. Note the progressive decrease in trabecular bone mass (*) with age in the mutant compared with wild-type mice. ***d***,***e***, Details of high resolution microradiographs of six-month-old animals. Note that the trabecular bone is reduced and extends over a shorter distance below the growth plate in the mutant bone (*e*). Also note that the angle between the femoral neck and the great trochanter (arrows) is wider in the mutant bone, a difference in shape that was consistently observed (*d*).

with supernumerary sex chromosomes present with increased limb length and high levels of *BGN* (ref. 11).

Mutant mice, compared with normal mice, show reduced bone mass that is apparent upon radiographic and microradiographic examination (Fig. 2). High-resolution radiographic images of entire long bones showed a reduction in the amount and density of trabecular bone, both in epiphyses and in metaphyses. Trabeculae were distributed over a shorter distance from the growth plate in the mutant mice compared with normal littermates. Cortical thickness was also reduced in mutant mice and the reduction in bone mass was easily detectable at three months and was even more prominent in six- and nine-month-old mutant mice. Subtle differences in bone shape, such as the wider angle between the femoral neck and the greater trochanter, could also be consistently detected in mutant bones (Fig. 2*d*).

The reduced bone mass in mutant mice was confirmed by histological analysis of both conventional and undecalcified plastic sections of femora, tibiae and vertebrae (Figs 3,4). Epiphyseal and metaphyseal trabecular structures of long bones were thinner, fewer and poorly connected to each other in the mutant bone (Fig. 3*a–f*). Similar changes in trabecular structures were also detected in vertebrae (Fig. 3*g*,*h*). In long bones, the cortical thickness of the diaphysis was also reduced (*Bgn*$^{-/0}$ 177.8 ± 5.7 μm, n = 3; *Bgn*$^{+/0}$ 218.2 ± 4.7 μm, n = 3; $P<0.01$; Fig. 3*i*,*j*). Established histomorphometric parameters estimating bone mass and bone cell numbers[12] were obtained by analysing undecalcified plastic sections of mutant and wild-type animals. Animals were labelled with tetracycline and calcein *in vivo* (Fig. 4) to measure the amount of bone deposited in the time interval defined by the administration of the two fluorescent markers.

BV/TV (bone volume/total tissue volume), a histomorphometric index of trabecular bone mass, was reduced to below 50% of normal values at three and nine months (Fig. 5*a*). The gain in bone mass observed between three and nine months (Δ BV/TV, Fig. 5*b*) as a function of skeletal growth was negligible in mutant mice, and significantly lower compared with normal littermates. As a result, the reduction in bone mass observed in mutant mice compared with normal littermates was progressively more obvious with increasing animal age. The osteoblast surface (ObS/BS,%, proportion of bone surfaces covered by osteoblasts), a reliable histomorphometric indicator of osteoblast numbers[12], was reduced in the mutant mice (Fig. 5*c*), whereas osteoclast surface (OcS/BS,%, proportion of bone surface covered by osteoclasts; Fig. 5*d*) and number (OcN/BS, number of osteoclast per bone surface unit; Fig. 5*e*) in mutant bones were equivalent to normal littermates. This suggested that the reduced bone mass was related to reduced bone formation and was not dependent upon increased osteoclastic bone resorption.

The decrease in bone formation was confirmed by measurement of established dynamic parameters of bone formation[12] in bone sections from animals that were dual labelled with tetracycline and calcein *in vivo* (Fig. 4). Mineralizing surface (MS, which estimates the proportion of bone surface undergoing mineralization, that is, the extent of formative surfaces; Fig. 5*f*), mineral apposition rate (MAR) and bone formation rate (BFR; both of which estimate, based on the spatial separation of the two fluores-

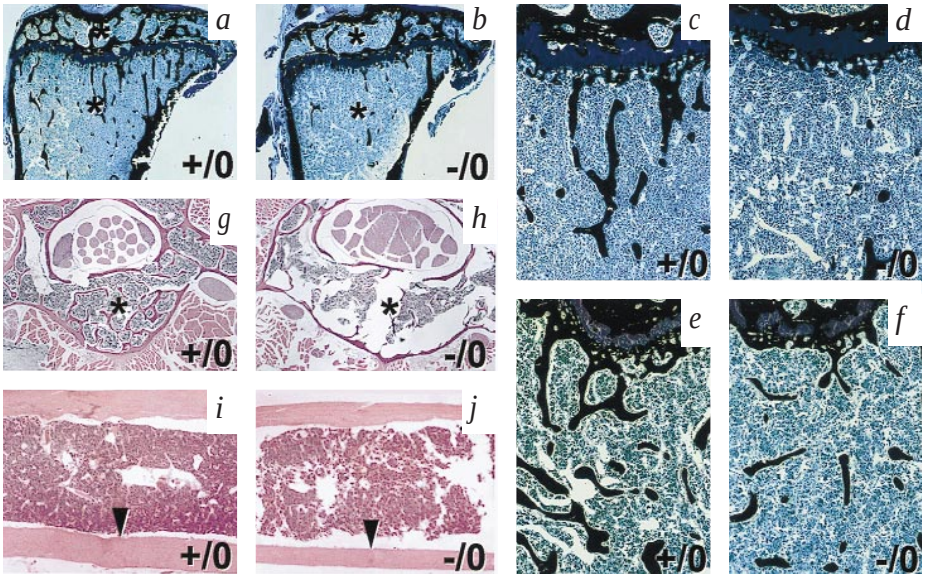

Fig. 3 Histological analysis of bones from *Bgn*$^{+/0}$ (0/+) and *Bgn*$^{-/0}$ (0/–) mice. ***a***,***b***, Low-power view of undecalcified plastic sections of the proximal tibia of six-month-old normal and mutant mice, stained with von Kòssa for mineral and counterstained with methylene blue. Trabecular structures are obviously reduced in the epiphysis and the metaphysis of mutant bone (asterisks). High-power views of undecalcified plastic sections of tibial metaphyses (***c***,***d***) of six-month-old normal and mutant mice further demonstrate the reduction in trabecular structures in mutant long bones, which can also be detected at three months in femoral metaphyses (***e***,***f***). ***g***,***h***, Trabecular bone in vertebrae of normal and mutant mice at six months showing a substantial decrease in the mutant compared with wild type. ***i***,***j***, At nine months, there was also cortical thinning (arrows) in mutant mice.

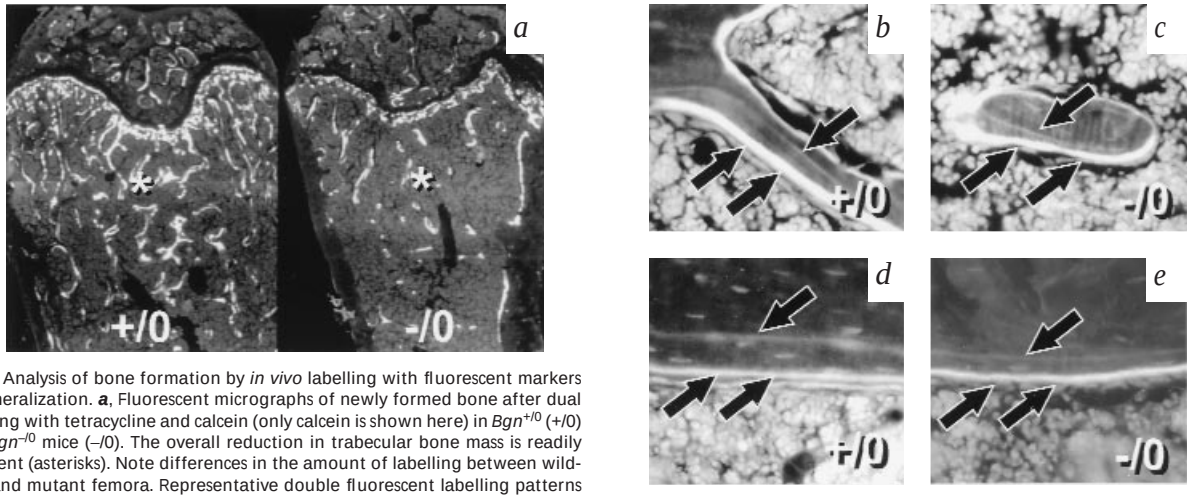

Fig. 4 Analysis of bone formation by *in vivo* labelling with fluorescent markers of mineralization. ***a***, Fluorescent micrographs of newly formed bone after dual labelling with tetracycline and calcein (only calcein is shown here) in $Bgn^{+/0}$ (+/0) and $Bgn^{-/0}$ mice (–/0). The overall reduction in trabecular bone mass is readily apparent (asterisks). Note differences in the amount of labelling between wild-type and mutant femora. Representative double fluorescent labelling patterns are shown for both trabecular (***b***,***c***) and cortical (***d***,***e***) bone of wild-type (+/0) and mutant animals (–/0) respectively. Note the differences in the distance between the tetracycline (faint label, single arrow) and calcein (vivid label, double arrows) labels. The distance represents the amount of bone which was deposited in the time interval between tetracycline and calcein administration.

cent labels in newly formed bone, the rate of bone formation during the time interval defined by the fluorescent labels; Fig. 5*g*,*h*) were all significantly decreased in mutant mice compared with normal littermates. Together, the static and dynamic histomorphometric measurements indicate that mutant mice reach a much lower maximal (peak) bone mass compared with normal littermates, due to deficient osteoblast numbers and activity.

Although total ash weight (an indicator of the mineral content for each bone) was reduced in mutant long bones ($Bgn^{-/0}$ 23.8 ± 2.7 mg/tibia, n = 7; $Bgn^{+/0}$ 29.8 ± 3.1 mg/tibia, n = 7; $P<0.01$), there was no significant reduction in bone ash content (mineral-to-matrix ratio: $Bgn^{-/0}$ 65.8 ± 1.2%, n = 7; $Bgn^{+/0}$ 66.8 ± 0.81%, n = 7). Furthermore, the mineral crystal size and shape as determined by X-ray diffraction (data not shown) was unaffected in mutant animals. However, when FTIRM (Fourier transform infrared microscopy) was used to measure the ratio of mineral (phosphate) to protein (amide) absorbance (which is related to the mineral-to-matrix ratio[13]), a decrease was observed in both trabecular mutant bone (three months: $Bgn^{-/0}$ 6.5 ± 2.3, n = 9; $Bgn^{+/0}$ 7.9 ± 1.4, n = 17; $P<0.05$; six months: $Bgn^{-/0}$ 6.39 ± 0.96, n = 20; $Bgn^{+/0}$ 7.77 ± 1.5, n = 11; $P<0.05$) and cortical mutant bone (three months: $Bgn^{-/0}$ 8.86 ± 1.4, n = 13; $Bgn^{+/0}$ 11.5 ± 1.5, n = 13; $P<0.05$; six months: $Bgn^{-/0}$ 7.86 ± 0.97, n = 24; $Bgn^{+/0}$ 9.48 ± 1.4, n = 24; $P<0.05$). These changes may reflect a localized effect of biglycan deficiency on mineral formation, as it has been reported that biglycan alters seed crystal growth and habit *in vitro*[14].

Biomechanical tests that primarily measure the structural and material properties of cortical bone[15] were carried out on three-,

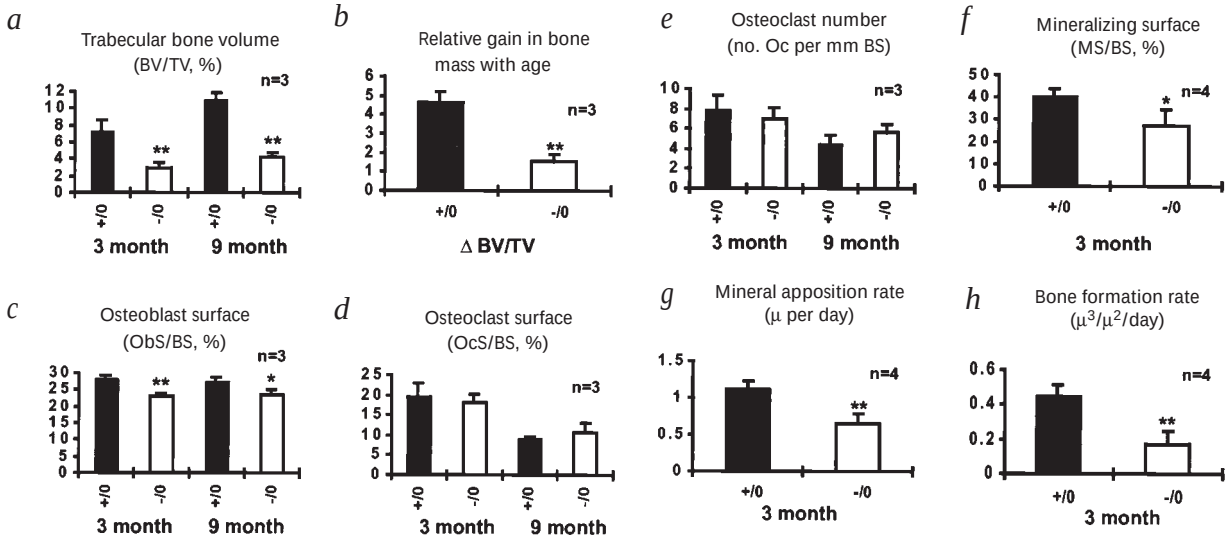

Fig. 5 Bone histomorphometry. ***a***, BV/TV represents the ratio of bone volume to tissue volume and estimates bone mass. ***b***, Δ BV/TV represents the gain in trabecular bone mass between three and nine months, and is calculated as the mean difference between BV/TV values recorded at nine months and the mean values of BV/TV at three months for each group (normal *versus* mutant). ***c***, ObS/BS,% represents the proportion of bone surface covered with osteoblasts, and estimates osteoblast numbers. OcS/BS,% (***d***) and OcN/BS (***e***) estimate bone resorption as osteoclast surface and number, respectively, over bone surface. MS (***f***), MAR (***g***) and BFR (***h***) are measured using sections from animals that were dual labelled with tetracycline and calcein *in vivo*. MS estimates the extent of bone surface undergoing mineralization (that is, formative bone surfaces). MAR and BFR measure the amount of bone that is mineralized or deposited per time unit, and are based on the measurement of the distance between the two fluorescent labels. Bars represent the mean ± s.d. for wild-type (closed) and mutant (open) mice, and * and ** indicate $P<0.05$ and $P<0.01$ between the two groups, respectively.

Table 1 • Biomechanical properties

Property	Genotype	3 mo	6 mo	9 mo
Yield energy (N mm)	+/0	33.52±5.76	25.28±3.99	19.39±3.17
	–/0	31.60±3.61	19.95±3.18*	17.16±3.57
Failure load (N)	+/0	38.46±6.02	36.29±9.96	33.85±6.44
	–/0	35.34±2.97	28.54±4.11**	28.18±6.55

Results using femora from three-month-old (mo) +/0 (n=5), –/0 (n=5), six-month-old +/0 (n=7), –/0 (n=9) and nine-month-old +/0 (n=5) –/0 (n=8) transgenic animals. Statistical significance between control and mutant animals was determined using two-way ANOVA (*P=0.017, **P=0.015).

six- and nine-month-old mouse femurs (Table 1). There was a trend towards decreased failure load (an indicator of bone strength) and yield energy (an indicator of bone ductility) in the mutant mice compared with normal mice. These data corroborate the histomorphometric analysis that indicate cortical thickness was less reduced (20%) compared with the reduction in trabecular bone volume (60–70%). Development of novel tests that specifically measure trabecular biomechanical properties (in mice) will be required for more detailed analysis of this specific pattern of osteoporosis and the performance of regions rich in trabecular bone, which are critical targets for osteoporotic fractures (for example, vertebrae).

Notably, osteoporosis-like phenotypes have been observed in other transgenic models, either as part of an accelerated senescence process (such as the klotho mouse, showing osteoporosis, reduced lifespan, skin atrophy, emphysema and infertility[16]) or as a result of an unbalanced local cytokine or growth factor milieu[17–19]. Most of the latter models reflect an induced increase in bone resorption/remodelling that mimics conditions of high turnover (type I) osteoporosis; that is, conditions whose hallmark is an acute loss of pre-existing bone[20]. For example, when TGF-β2 was over-expressed in osteoblasts, a low bone mass developed as a result of increased bone remodelling[18], indicating that TGF-β2 is a critical factor in the control of bone remodelling. Overexpression of G-CSF (known to control osteoclast differentiation) stimulated bone resorption[19], and ablation of osteoprotegerin, an inhibitor of osteoclast formation, also resulted in severe and early onset osteoporosis[21], apparently due to unabated osteoclast formation. In contrast, over-expression of IL-4 in T-cells resulted in a low bone mass associated with a reduced level of bone turnover[17]. The *Bgn* line we have generated develops an osteoporosis-like phenotype as a result of reduced bone formation and inadequate gain in bone mass during bone growth. Peak bone mass, achieved by skeletal growth, is the most critical risk factor for human osteoporotic syndromes, and is the single pathogenetic factor of osteoporotic diseases for which the influence of genetic determinants is considered critical. To date, the complete list of genes controlling the level of peak bone mass have not been delineated. Mutations in the type I collagen genes (the predominant structural protein in bone matrix), have been postulated to result in certain forms of human osteoporosis that are at the 'borderline' with concealed forms of mild osteogenesis imperfecta[22]. Deletions of two other connective tissue genes that are highly expressed in bone (decorin and osteonectin) have failed to result in a detectable skeletal phenotype[23,24], whereas ablation of the osteocalcin gene (a non-collagenous protein unique to bone matrix) resulted in a phenotype characterized by increased bone mass and increased bone formation[25]. Thus, *Bgn* is the first non-collagenous matrix protein found in bone that acts as a positive regulator of bone formation and bone mass, and indicates that at least one member of the proteoglycan family of genes (which encode components that may have a role in matrix organization) controls bone mass by significantly affecting the cellular process of bone formation.

Methods

Gene targeting. A 129Sv mouse genomic library (Stratagene™) was screened with a rat *Bgn* cDNA probe. A 4.3-kb fragment of mouse *Bgn* containing the coding sequence of exons 2–5 was used to construct a targeting vector. *Bgn* was disrupted by inserting the PGK-*neo* cassette from the pPNT vector[26] into exon 2 at the *Tth*111I site. The PGK-TK cassette was used for negative selection[26]. J1 ES cells[27] were transfected with linearized targeting vector (50 μg per 1.5×10^7 cells) using a BioRad Gene Pulser™ and grown under double selection (350 μg/ml G418, 2 μM gancyclovir) as described[28]. Targeted ES cell clones were identified by Southern-blot hybridization and injected into C57BL/6 blastocysts to generate chimaeras[29]. Overt chimaeras were crossed with C57BL/6 mice to produce germline transmission of the targeted allele.

RNA and protein analysis. Western-blot analysis was performed with a SuperSignal™ western-blot kit (Pierce) using antibody LF-106 for biglycan and LF-113 for decorin[30]. RNA (10 μg) was separated on an agarose formaldehyde gel and hybridized with a labelled mouse *Bgn* cDNA probe[3].

Radiographic analysis. Bones were dissected free of soft tissues and subjected to x-ray analysis using a Faxitron MS-20 specimen radiography system (Faxitron X-ray) and microradiographs were prepared using an XRG 3000 (Ital Structures) x-ray generator, both using high resolution film (Kodak).

Histology. Bones were fixed in paraformaldehyde (4%) for 16–24 h. Samples were demineralized for 7–10 d in EDTA (10%), dehydrated, embedded in paraffin, sectioned (5 μm) and stained with haematoxylin and eosin. For bone histomorphometry, samples were processed undecalcified and embedded in either methyl methacrylate or glycol methacrylate. Sections were stained with methylene blue/Azur II, Giemsa and von Kòssa. For *in vivo* fluorescent labelling, a single intraperitoneal injection of tetracycline (25 mg/kg body weight) was administered at day 0, and a single intraperitoneal injection of calcein at the same dose was administered at day 10. Animals were killed at day 12 (ref. 31). Bones dissected from *in vivo* labelled animals were fixed in paraformaldehyde (4%) and embedded in methyl methacrylate. For each sample, four unstained non-consecutive sections (10 μm) were analysed by histomorphometry using fluorescence microscopy. All histomorphometric measurements were made blindly on trabecular bone of the femoral metaphysis, using a microscope equipped with a TV camera interfaced to a computer running custom-designed software for bone histomorphometry (IAS 2000, Delta Systems). Bone resorption parameters (osteoclast number and surface) were measured by counting the number and surface of tartrate-resistant acid-phosphatase–positive cells[32,33]. All histomorphometric parameters are reported in accordance with the recommended ASBMR nomenclature[12]. Δ BV/TV represents the gain in trabecular bone mass between three and nine months, and is calculated as the mean difference between BV/TV values recorded at nine months and the mean values of BV/TV at three months for each group (normal *versus* mutant). Statistical analysis was performed by one-way ANOVA with student t-test for comparison.

Biomechanics. The biomechanical properties of the bones were tested for bone strength as measured by the property 'failure load' and for bone flexibility as measured by the property 'yield energy'. Biomechanical tests were performed as described[15]. Briefly, whole femora were loaded to failure in a 4-point bending test on a servohydraulic system at a constant displacement rate of 0.5 mm/s until failure occurred.

Acknowledgements

We thank D. Caden and M. Mankani for X-ray analysis, D. Porter for advice with gene targeting vector and D. Eanes, N. Marino, D. Paget, J. Liang and S. Dieúdonne for help with the project.

Received 19 February; accepted 29 July, 1998.

1. Fisher, L.W. *et al.* Proteoglycans of developing bone. *J. Biol. Chem.* **258**, 6588–6594 (1983).
2. Bianco, P., Fisher, L.W., Young, M.F., Termine, J.D. & Robey, P.G. Expression and localization of the two small proteoglycans biglycan and decorin in developing human skeletal and non-skeletal tissues. *J. Histochem. Cytochem.* **38**, 1549–1563 (1990).
3. Fisher, L.W., Termine, J.D. & Young, M.F. Deduced protein sequence of bone small proteoglycan I (biglycan) shows homology with proteoglycan II (decorin) and several nonconnective tissue proteins in a variety of species. *J. Biol. Chem.* **264**, 4571–4576 (1989).
4. Schönherr, E. *et al.* Interaction of biglycan with type I collagen. *J. Biol. Chem.* **270**, 2776–2783 (1995).
5. Yamaguchi, Y., Mann, D.M. & Ruoslahti, E. Negative regulation of transforming growth factor-beta by the proteoglycan decorin. *Nature* **346**, 281–284 (1990).
6. Hildebrand, A. *et al.* Interaction of the small interstitial proteoglycans biglycan, decorin and fibromodulin with transforming growth factor beta. *Biochem. J.* **302**, 527–534 (1994).
7. Kappler, J. *et al.* Chondroitin/dermatan sulphate promotes the survival of neurons from rat embryonic neocortex. *Eur. J. Neurosci.* **9**, 306–318 (1997).
8. Iozzo, R.V. & Murdoch, A.D. Proteoglycans of the extracellular environment: clues from the gene and protein side offer novel perspectives in molecular diversity and function. *FASEB J.* **10**, 598–614 (1996).
9. Ruoslahti, E. Proteoglycans in cell regulation. *J. Biol. Chem.* **264**, 13369–13372 (1989).
10. Ruoslahti, E. & Yamaguchi, Y. Proteoglycans as modulators of growth factor activities. *Cell* **64**, 867–869 (1991).
11. Vetter, U.K. *et al.* in *Basic and Clinical Approach to Turner Syndrome* (eds Hibi, I. & Takano, K.) 143–146 (Elsevier, Amsterdam,1993).
12. Parfitt, A.M. *et al.* Bone histomorphometry: standardization of nomenclature, symbols, and units. Report of the ASBMR Histomorphometry Nomenclature Committee. *J. Bone Miner. Res.* **2**, 595–610 (1987).
13. Boskey, A.L., Pleshko, N., Doty, S. & Mendelsohn, R. Applications of Fourier Transform InfraRed (FT-IR) microscopy to the study of mineralization in bone and cartilage. *Cells & Materials* **2**, 209–220 (1992).
14. Boskey, A.L., Spevak, L., Doty, S.B. & Rosenberg, L. Effects of bone CS-proteoglycans, DS-decorin, and DS-biglycan on hydroxyapatite formation in a gelatin gel. *Calcif. Tissue Int.* **61**, 298–305 (1997).
15. Bonadio, J. *et al.* A murine skeletal adaptation that significantly increases cortical bone mechanical properties. Implications for human skeletal fragility. *J. Clin. Invest.* **92**, 1697–1705 (1993).
16. Kuro-o, M. *et al.* Mutation of the mouse *klotho* gene leads to a syndrome resembling aging. *Nature* **390**, 45–51 (1997).
17. Lewis, D.B. *et al.* Osteoporosis induced in mice by overproduction of interleukin 4. *Proc. Natl Acad. Sci. USA* **90**, 11618–11622 (1993).
18. Erlebacher, A. & Derynck, R. Increased expression of TGF-beta 2 in osteoblasts results in an osteoporosis-like phenotype. *J. Cell Biol.* **132**, 195–210 (1996).
19. Takahashi, T., Wada, T., Mori, M., Kokai, Y. & Ishii, S. Overexpression of the granulocyte colony-stimulating factor gene leads to osteoporosis in mice. *Lab Invest.* **74**, 827–834 (1996).
20. Riggs, B.L. & Melton, L.J. 3rd. Involutional osteoporosis. *N. Engl. J. Med.* **314**, 1676–1686 (1986).
21. Bucay, N. *et al.* osteoprotegerin-deficient mice develop early onset osteoporosis and arterial calcification. *Genes Dev.* **12**, 1260–1268 (1998).
22. Prockop, D.J. & Kivirikko, K.I. Collagens: molecular biology, diseases, and potentials for therapy. *Annu. Rev. Biochem.* **64**, 403–434 (1995).
23. Danielson, K.G. *et al.* Targeted disruption of decorin leads to abnormal collagen fibril morphology and skin fragility. *J. Cell Biol.* **136**, 729–743 (1997).
24. Gilmour, D.T. *et al.* Mice deficient for the secreted glycoprotein SPARC/osteonectin/BM40 develop normally but show severe age-onset cataract formation and disruption of the lens. *EMBO J.* **17**, 1860–1870 (1998).
25. Ducy, P. *et al.* Increased bone formation in osteocalcin-deficient mice. *Nature* **382**, 448–452 (1996).
26. Tybulewicz, V.L., Crawford, C.E., Jackson, P.K., Bronson, R.T. & Mulligan, R.C. Neonatal lethality and lymphopenia in mice with a homozygous disruption of the c-abl proto-oncogene. *Cell* **65**, 1153–1163 (1991).
27. Li, E., Bestor, T.H. & Janeisch, R. Targeted mutation of the DNA methyl transferase gene results in embryonic lethality. *Cell* **69**, 915–926 (1992).
28. Love, P.E., Tremblay, M.L. & Westphal, H. Targeting of the T-cell receptor zeta-chain gene in embryonic stem cells: strategies for generating multiple mutations in a single gene. *Proc. Natl Acad. Sci. USA* **89**, 9929–9933 (1992).
29. Bradley, A. in *Teratocarcinomas and Embryonic Stem Cells* (ed. Robinson, E.J.) 113–151 (IRL, Oxford, 1987).
30. Fisher, L.W., Stubbs, J.T. Jr. & Young, M.F. Antisera and cDNA probes to human and certain animal model bone matrix noncollagenous proteins. *Acta Orthop. Scand. Suppl.* **266**, 61–65 (1995).
31. Vignery, A. & Baron, R. Dynamic histomorphometry of alveolar bone remodeling in the adult rat. *Anat. Rec.* **196**, 191–200 (1980).
32. Boyce, B.F., Yoneda, T., Lowe, C., Soriano, P. & Mundy, G.R. Requirement of pp60*c-src* expression for osteoclasts to form ruffled borders and resorb bone in mice. *J. Clin. Invest.* **90**, 1622–1627 (1992).
33. Andersson, G. & Ek-Rylander, B. The tartrate-resistant purple acid phosphatase of bone osteoclasts—a protein phosphatase with multivalent substrate specificity and regulation. *Acta Orthop. Scand. Suppl.* **266**, 189–194 (1995).